Annals of Anatomy 225 (2019) 33–41

Contents lists available at ScienceDirect

Annals of Anatomy

journal homepage: www.elsevier.com/locate/aanat

RESEARCH ARTICLE

Craniofacial abnormalities in a murine model of Saethre-Chotzen Syndrome

Sarah Lonsdale[a], Robin Yong[a], Alexander Khominsky[a], Suzanna Mihailidis[a], Grant Townsend[a], Sarbin Ranjitkar[a,*,1], Peter J. Anderson[a,b,c,*,1]

[a] Adelaide Dental School, The University of Adelaide, Adelaide, SA 5000, Australia
[b] Australian Craniofacial Unit, Women's and Children's Hospital, 72 King William St., North Adelaide, SA 5006, Australia
[c] South Australian Health and Medical Research Institute (SAHMRI), Adelaide, SA 5000, Australia

ARTICLE INFO

Article history:
Received 25 March 2019
Received in revised form 19 May 2019
Accepted 28 May 2019

Keywords:
Craniosynostosis
Craniofacial phenomics
Maxilla
Mandible
Tooth

ABSTRACT

Background: Saethre-Chotzen Syndrome (SCS) is an autosomal dominant syndrome that occurs due to a mutation or deletion of the *Twist1* gene at chromosome 7p21. Our aim was to conduct a morphometric analysis of the craniofacial features in the mouse associated with a Twist1$^{+/-}$ mutation.
Methods: Micro-computed imaging was conducted for the skulls of forty skeletally mature mice, equally distributed by sex (male and female) and two genotypes (Twist1$^{+/-}$ or murine model of SCS; and Twist1$^{+/+}$ or wild-type). A morphometric analysis was carried out for eight parameters for the maxillary-zygomatico-temporal region, 10 parameters for the mandible and three parameters for teeth from three-dimensional reconstructions.
Results: Compared with wild-type, the murine model of SCS showed these trends: (1) *maxillary-zygomatico-temporal region*, significantly shorter length and width posteriorly ($p < 0.05$), (2) *mandible*, significantly reduced height and width ($p < 0.05$), and (3) *teeth*, significantly shorter height, shorter mesio-distal width but longer bucco-lingual width ($p < 0.05$). In the murine model of SCS, the key morphological variations included incomplete ossification of the temporal bone and zygomatic arch, twisting and/or incomplete ossification of the palatal process of the maxilla, premaxilla and the ventral nasal concha, as well as bifid coronoid processes.
Conclusions: The skeletal and dental alterations in the height, length and width provide a foundation for large-scale phenomics studies, which will improve existing knowledge of the Twist1 signalling cascade. This is relevant given the predicted shift towards minimally invasive molecular medical treatment for craniosynostosis.

1. Introduction

Saethre-Chotzen Syndrome (SCS) is an autosomal dominant craniofacial syndrome characterized by unilateral or bilateral coronal craniosynostosis (the premature fusion of cranial suture/s), facial dysmorphia and limb abnormalities (Anderson et al., 1996; Wang et al., 2016). Severe cases of SCS can be associated with cognitive impairment, psychosocial issues and sensory disorders, including vision and hearing impairment (Woods et al., 2009). Treatment may require multiple surgeries to correct craniosynostosis during early childhood, followed by the correction of facial disproportion during adolescence (Taylor and Bartlett, 2017).

SCS occurs due to a loss of function mutation, or complete deletion of the Twist1 gene (localized to chromosome 7p21), which encodes a basic helix loop helix (BHLH) transcription factor (protein) (Kress et al., 2006). As in the case of investigating genetic mutation in human diseases, murine models have been critical in understanding both the normal physiology and underlying pathogenesis of SCS. Compared to human models, murine models have the added benefits of high reproductive rates, low cost of upkeep and are in plentiful supply. Most importantly, they are invaluable in ensuring controlled conditions by enabling a consistent genetic basis to localize the effects of a gene, and to understand the phenotypes linked to human disease states. Murine model of SCS can isolate the effect of Twist1 by utilizing a heterozygous model

* Corresponding author at: Adelaide Dental School, University of Adelaide, Adelaide Health and Medical Sciences Building, Cnr George St. and North Tce, Adelaide, SA 5000, Australia.
E-mail addresses: sarbin.ranjitkar@adelaide.edu.au (S. Ranjitkar), haemro2@hotmail.com (P.J. Anderson).
[1] Equal last author contribution.

https://doi.org/10.1016/j.aanat.2019.05.011
0940-9602/

(Twist1$^{+/-}$) or conditional gene inactivation to overcome the early embryonic lethality of double knockout, homozygous (Twist1$^{-/-}$) mutation (Chen and Behringer, 1995). Homology between human and murine Twist1 proteins has been established, and the existing murine Twist1$^{+/-}$ model reflects phenotypes that are consistent with the human SCS (Carver et al., 2002; El Ghouzzi et al., 1999).

Twist mRNA is expressed in the cranial mesoderm and neural crest cells (NCCs), and the limb mesenchyme (Bildsoe et al., 2009), making it an essential mediator in the morphogenesis of the cranium and the limb through its contribution to the formation of germ cells layers, lineage commitment, maintenance of boundary integrity and behavior of osteogenic cells (Morriss-Kay and Wilkie, 2005; Twigg and Wilkie, 2015). During the early stages of facial development, NCCs migrate to various targets in the face including the bones via complex interactions with the head ectoderm, mesoderm and endoderm (Flaherty et al., 2016). In mutant mice, loss of function of the Twist1 transcription factor has different effects on the cranial mesoderm compared to NCCs, which has been attributed to the regulation of different genes via the two cell populations (Bildsoe et al., 2016). Ultimately, loss of function of Twist1 in the craniofacial region dysregulates molecular controls essential for normal craniofacial morphogenesis, resulting in cranial dysmorphology and associated comorbidities (Bildsoe et al., 2016; O'Rourke and Tam, 2004).

Although research in craniosynostosis and the skull is well-documented, literature specific to the maxilla, mandible and teeth is limited to case reports and cohort studies which provide only observational or qualitative information. Compared with the wild-type murine model, maxillary phenotypical differences observed in Twist1 models include hypoplasia and a cleft or high-arched palate (Epstein et al., 2004; Stoler et al., 2009). Mandibular hypoplasia, impaired ramal development and altered mandibular shape have also been observed (Zhang et al., 2012). During tooth development, Twist1 gene plays a role in early cell proliferation, odontoblast differentiation and FGF signalling in the dental mesenchyme (Meng et al., 2015). Given that the maxilla, the mandible, the temporal bone (including the posterior part of the zygomatic arch) and teeth are important components of functional occlusion, and that the morphological changes in one component can cause adaptive changes in other component(s), it is important to characterize these morphological structures in various health and disease states. To our knowledge, there is currently no comprehensive analysis of the effects of Twist1 mutation on the maxillary-zygomatico-temporal region (which incorporates the posterior part of the zygomatic arch), mandible and teeth.

Our aims were (i) to characterize the craniofacial features quantitatively, specifically for the maxillary-zygomatico-temporal region, mandible and teeth, in murine models of SCS (Twist1$^{+/-}$) and wild-type (Twist1$^{+/+}$) at skeletal maturity (at 3.0–3.5 months of age), and (ii) to qualitatively assess craniofacial features that may be unique to this murine model. Given that a heterozygous loss of Twist1 affects the whole craniofacial skeleton through a brachycephalic tendency (Parsons et al., 2014), we hypothesised that the maxillary-zygomatico-temporal region and mandible in a murine model of SCS (Twist1$^{+/-}$) would be significantly smaller compared with the wild-type.

2. Materials and methods

Ethics approval was obtained from the University of Adelaide and the Women's and Children's Health Network (WCHN) Animal Ethics Committee (AEC 1001) (approval number 1000/8/2018).

2.1. Animal husbandry

Twist1$^{+/-}$ mice and wild-type (Twist1$^{+/+}$) mice were donated by Professor Stan Gronthos from the South Australian Health and Medical Research Institute. The mice were preserved on a mixed Swiss/C57BL genetic background. As the C57BL mice were poor breeders, they were bred with Swiss mice to keep the colony robust. However, there is no evidence of discernible difference in gene expression between these two strains. They were housed at the Women's and Children's Hospital (Adelaide, Australia) with food and water ad libitum.

2.2. Samples

Forty skeletally mature mice (3.0–3.5 months old) were used in this study, equally distributed between the two genotypes (murine model of SCS (Twist1$^{+/-}$) and wild-type (Twist1$^{+/+}$)) and the sexes (male and female) (n = 10 in each group). The sample calculation of 10 per group has been shown to provide adequate power for this type of study (Khominsky et al., 2018). Euthanasia was carried out by CO_2 asphyxiation, followed by cervical dislocation. The skulls (with soft tissues intact) were stored in formalin for the duration of the study.

2.3. Micro-CT imaging and 3D reconstruction

The whole murine skulls (with intact soft tissues) were subjected to micro-computed tomography (micro-CT) scanning using a SkySkan 1076 small animal micro-CT scanner (Bruker; Kontich, Belgium) housed at Adelaide Microscopy. All skulls were scanned at a resolution of 8.65 μm, using established parameters as described by Mian et al. (2017): source voltage: 74 kV, source current: 135 μA, rotation step: 0.8, filter: 0.5 A and exposure time: 1767 ms. Cross-sectional image slices were then reconstructed with the SkyScan NRecon software package (Bruker, Kontich, Belgium) with a smoothing of 3 pixels, misalignment compensation <2.0, ring artefact correction of 10, beam hardening correction of 30%, and upper and lower thresholding limits of 0.0 and 0.11 respectively. The bitmap image slices were loaded into Mimics Innovation Suite 18.0 software (Materialise, Leuven, Belgium) and 3D models were rendered. Thresholding was applied to separate the soft tissues from the bony elements. MeshLab, an Open-Source Mesh Processing Tool 64bit v1.3.3 (Cignoni et al., 2008) was used for 3D morphometric analysis.

Micro-CT images showed craniosynostosis in all the mutant (Twist1$^{+/-}$) mice, including coronal synostosis in 14 (70.0%), sagittal synostosis in 4 (20.0%) and both coronal and sagittal synostosis in 2 (10.0%) mice. Craniosynostosis was not observed in any wild-type mouse.

2.4. Morphometric analysis

One examiner (S.L.) was blinded during all stages of morphometric analysis. Landmarks for the maxillary-zygomatico-temporal region, mandible and teeth were adapted from previous craniofacial morphometric studies (Khominsky et al., 2018; Richtsmeier et al., 2000). Maxillary-zygomatico-temporal region and mandibular morphology were compared between the two samples of mice using eight and 10 linear dimensions respectively; and dental morphology was compared using three linear crown measurements for both the maxillary and mandibular first molars. The landmarks are summarized in Table 1, Fig. 1(a–c) and Fig. 2(a–d).. Reproducible landmarks were obtained by orientating the occlusal table of the maxilla and mandible parallel to the true horizontal plane. As the whole skulls were scanned, the fibrous joint between the hemi-mandibles remained intact and enabled

Table 1
Landmarks used in the craniofacial morphometric analysis for the maxillary-zygomatico-temporal region (Mx), mandible (Mn) and first molar teeth between wild-type (Twist1$^{+/+}$) and murine model of SCS (Twist1$^{+/-}$).

Landmarks	Description of landmarks
Maxillary-zygomatico-temporal region	
Maximum height	Coincidence of premaxilla, maxilla and maxillary fossa (PMMF) — coincidence of premaxilla, maxilla and frontal (PMF)
Total length	Anterior nasal spine (ANS) — maxilla (M), at the most posterior point
Anterior length	Anterior nasal spine (ANS) — coincidence of premaxilla, maxilla and midpalatine suture (PMM)
Posterior length	Coincidence of premaxilla, maxilla and midpalatine suture (PMM) — maxilla (M), at the most posterior point
Anterior width	Intersection of frontal process of maxilla with frontal and lacrimal bones (MFL)
Middle width: inter-anterior zygomatic	Zygomatic process of maxilla (AZyg), at the most anterior point
Posterior width inter-maxillary tuberosity	Maxillary tuberosity (MT), at the most lateral and posterior point
Posterior width: inter-zygomatic process of squamosal width	Zygomatic process of the squamosal (ZS), at the most posterior point
Mandible	
Ascending height	Coronoid process (Cp), at the most superior point — gonion (Go)
Descending height	Coronoid process (Cp), at the most superior point — menton (Me)
Anterior height	Menton (Me) — mandibular alveolar point (MAP)
Posterior height	Gonion (Go) — most anterior point of the condyle (Co)
Mandibular length	Gonion (Go) — pogonion (Pg)
Anterior width: inter-incisive	Lateral incisor alveolar rim (LIAR), at the most superior point
Middle width: inter-masseteric ridge	Masseteric ridge (MR), at the most anterior point
Posterior width: inter-coronoid	Coronoid process (Cp), at the most superior point
Posterior width: inter-condylar	Condyle (Co), at the most anterior point
Posterior width: inter-gonial width	Gonion (Go)
Dental	
Maxilla	
Height: CEJ–MB cusp tip (buccal view)	Maximum height from the CEJ to MB cusp tip
Length: Mesio-distal (buccal view)	Mesial to distal proximal surface at maximum convexity
Width: Bucco-palatal (occlusal view)	Widest part of the occlusal table from the buccal to the lingual surfaces along the marginal ridge
Mandible	
Height: CEJ–ML cusp tip (lingual view)	Maximum height from the CEJ to ML cusp tip
Length: mesio-distal (lingual view)	Mesial to distal proximal surface at maximum convexity
Width: bucco-lingual (occlusal view)	Widest part of the occlusal table from the buccal to the lingual surfaces along the marginal ridge

Abbreviations: Mx, maxilla; Mn, mandible; CEJ, cementoenamel junction; MB, mesiobuccal; ML, mesiolingual.
Transverse dimensions were measured from left to right between the landmarks described.

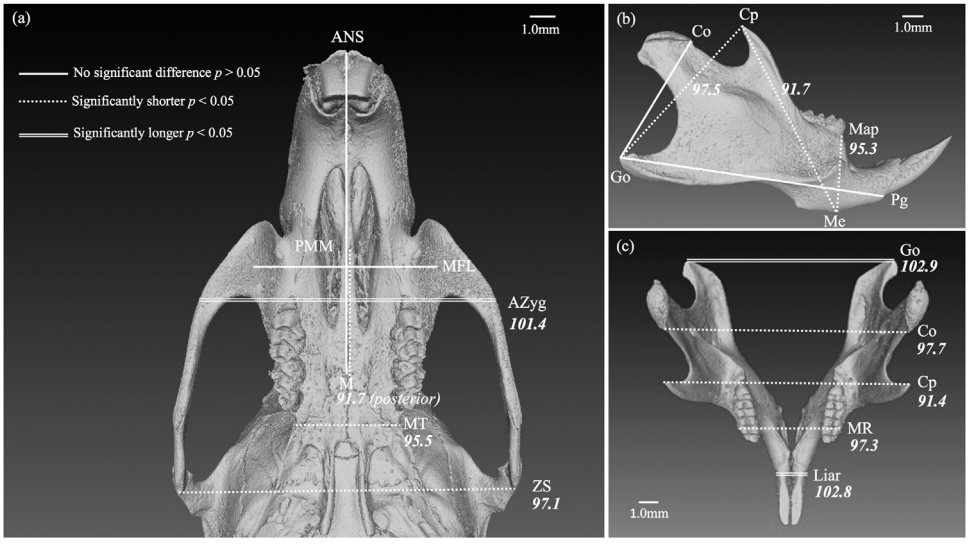

Fig. 1. Murine morphometric analysis of murine model of SCS (Twist1$^{+/-}$) compared with wild-type (Twist1$^{+/+}$) in 3D micro-CT reconstructions for the maxillary-zygomatico-temporal region from ventral view (a), and mandible from both lateral and dorsal views (b, c). Large dashes represent a statistically significant increase in size, and small dashes represent a statistically significant decrease in size at $p < 0.05$. An uninterrupted line demonstrates there was no significant difference. The numbers adjacent to the landmarks represent the mean ratio of the Twist1$^{+/-}$ and Twist1$^{+/+}$ mice. Definitions of the abbreviations are outlined in Table 1.

the widths of the whole mandible to be measured. Qualitative analysis was carried out by observing all views of the maxillary-zygomatico-temporal region and mandible (ventral, dorsal, lateral, caudal and cranial) to identify any phenotypical deviations from normal.

2.5. Statistical analysis

Statistical analysis was performed using the IBM SPSS Statistics package (version 25) (International Business Machines Corp, Armonk, New York, United States). Multivariate analysis of vari-

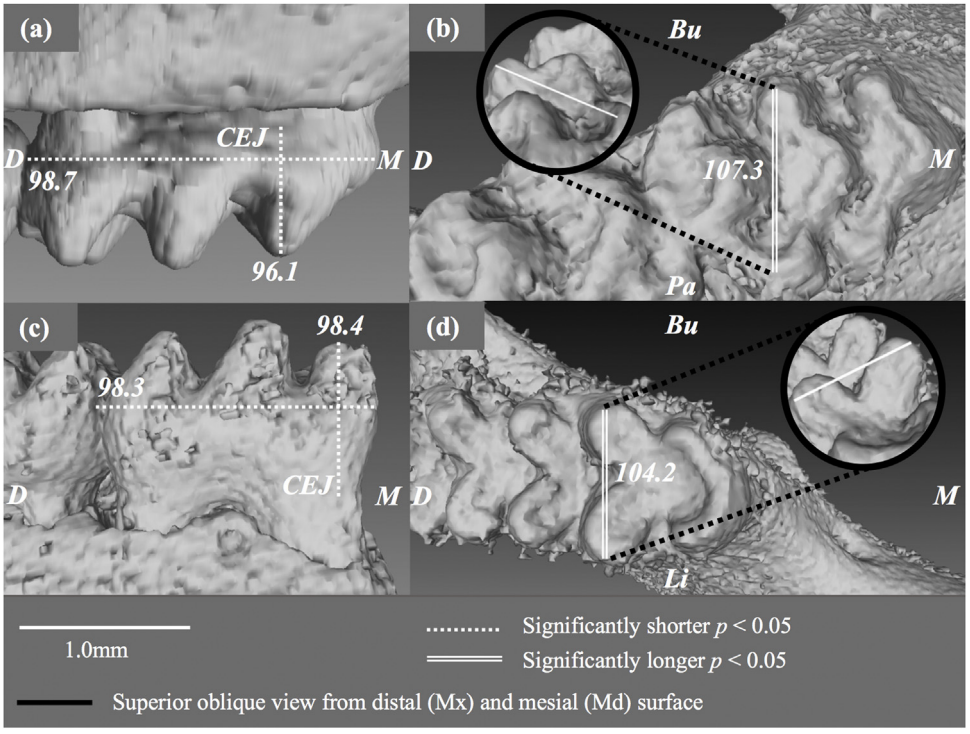

Fig. 2. Murine morphometric analysis of murine model of SCS (Twist1$^{+/-}$) compared with wild-type (Twist1$^{+/+}$) mice for maxillary (a–b) and mandibular (c–d) first molars. Large dashes represent a statistically significant increase in size, and small dashes represent a statistically significant decrease in size at $p < 0.05$. An uninterrupted line demonstrates there was no significant difference. The numbers adjacent to the landmarks represent the mean ratio of the SCS (Twist1$^{+/-}$) mice relative to the wild-type (Twist1$^{+/+}$) mice. To enable a comparison between the maxilla and mandible the diagram reflects the mean ratio and scale separated for each jaw. However, the maxillary and mandibular data was combined for statistical analysis, with the combined ratios as follows: *(i)* height 97.2%, *(ii)* length 98.5% and *(iii)* width 105.8%. Definitions of the abbreviations are outlined in Table 1.

ance (MANOVA) was conducted for each jaw separately (maxilla and mandible), and combined together for teeth, to assess whether there were significant differences in measurements between the genotypes and sexes. The data were pooled for left and right sides because there were no systematic differences between them. The effect-size (Cohen's f) data was calculated by using the formula: $f = \sqrt{(\eta 2/(1 - \eta 2))}$, where $\eta 2$ (partial ita-squared) was obtained as MANOVA output. The effect size (f) of 0.10 is mild, 0.25 is moderate and 0.40 is high. Statistical significance was set at $p < 0.05$.

2.6. Reliability

All measurements were repeated by the same examiner (S.L.) two weeks apart. Intra-examiner reliability was carried out as described by Harris and Smith (2009), and as previously applied in murine studies by Khominsky et al. (2018) and Mian et al. (2017). Paired t-tests (2-tailed) showed no significant systematic error ($p > 0.05$). High intra-examiner reliability was confirmed with the relative technical error of measurement for all parameters being <1.7%.

2.7. Dissection

Dissection was carried out in the laboratories at the Women's and Children's Hospital on murine model of SCS under 20× magnification and lighting when micro-CT scans demonstrated gross malformation of cranial bones.

3. Results

3.1. Maxillary-zygomatico-temporal region

The descriptive statistics for the maxillary-zygomatico-temporal parameters are summarised in Table 2 and Fig. 1(a). Two-way MANOVA showed a significant effect of genotype (Twist1$^{+/+}$ vs Twist1$^{+/-}$) (Wilks' $\lambda = 0.33$, hypothesis df = 8, error df = 29, F = 7.26, $p < 0.001$) and sex (males vs females) (Wilks' $\lambda = 0.57$, hypothesis df = 9, error df = 29, F = 2.76, $p < 0.05$) on the maxillary-zygomatico-temporal parameters. Compared with the wild-type, the Twist1$^{+/-}$ mice displayed these trends in the maxillary-zygomatico-temporal region: *(i) height*: no significant difference ($p > 0.05$); *(ii) length*: unaltered total and anterior lengths ($p > 0.05$), and significantly shorter posterior length (91.7% at $p < 0.01$); *(iii) width*: unaltered anterior width ($p > 0.05$), significantly longer middle (inter-anterior zygomatic) width (101.4% at $p < 0.05$), and significantly shorter posterior widths (including inter-maxillary tuberosity width, 95.5% at $p < 0.001$; and inter-zygomatic process of squamosal width, 97.1% at $p < 0.001$). The maxillary-zygomatico-temporal region was significantly longer in males compared with females for maximum height (102.6% at $p < 0.01$), but there was no significant difference in any other dimension. The effect size values for significant differences noted for the maxillary-zygomatico-temporal region were large for both the genotype (0.38 to 0.67) and sex (0.57) (Table 2).

Fig. 3(a–i) shows incidental phenotypical observations for the craniofacial region in the temporal bone, zygomatic arch, and palatal process of the maxilla, premaxilla and the ventral nasal concha. The micro-CT scans demonstrated missing mastoid and tympanic processes of the temporal bone and areas of the zygo-

Table 2
Comparison of various measurements in millimetres (mm) for the maxillary-zygomatico-temporal region (Mx), mandible (Mn) and first molar teeth between wild-type (WT) (Twist1$^{+/+}$) and murine model of SCS (Twist1$^{+/-}$).

Dimensions	Wild-type (WT)				Saethre-Chotzen Syndrome (SCS)				Effect-size (Cohen's f) (significance level in brackets)		
	Male (M)		Female (F)		Male (M)		Female (F)		SCS v WT	M v F	Mx vs Mn
	Mean	SD	Mean	SD	Mean	SD	Mean	SD			
Skeletal feature: maxillary-zygomatico-temporal region									1.42 ($p < 0.001$)	0.87($p < 0.05$)	–
Maximum height	5.54	0.13	5.38	0.09	5.53	0.11	5.41	0.18		0.57 ($p < 0.01$)	–
Total length	11.41	0.19	11.07	0.60	11.05	0.57	10.99	0.60			–
Anterior length	6.61	0.19	6.43	0.30	6.22	0.47	6.40	0.46			–
Posterior length	4.78	0.12	4.66	0.39	4.23	0.41	4.42	0.45	0.57 ($p < 0.01$)		–
Anterior width	7.42	0.09	7.34	0.15	7.30	0.21	7.35	0.34			–
Middle width: inter-anterior zygomatic	12.45	0.20	12.37	0.16	12.67	0.29	12.49	0.26	0.38 ($p < 0.05$)		–
Posterior width: inter-maxillary tuberosity	4.13	0.12	4.22	0.07	4.01	0.17	3.96	0.17	0.73 ($p < 0.001$)		–
Posterior width: inter-zygomatic process of squamosal	14.24	0.16	14.23	0.22	13.84	0.34	13.81	0.48	0.67 ($p < 0.001$)		–
Skeletal feature: mandible									2.03 ($p < 0.001$)	1.42 ($p < 0.001$)	–
Ascending height	7.71	0.16	7.39	0.22	7.53	0.30	7.20	0.33	0.38 ($p < 0.05$)	0.66 ($p < .001$)	–
Descending height	10.51	0.18	10.53	0.23	9.58	0.43	9.71	0.72	1.04 ($p < 0.001$)		–
Anterior height	3.71	0.08	3.68	0.08	3.56	0.08	3.48	0.16	0.86 ($p < 0.001$)		–
Posterior height	5.97	0.13	5.74	0.16	5.93	0.30	5.59	0.30		0.64 ($p < 0.001$)	–
Mandibular length	13.06	0.21	12.74	0.35	12.87	0.26	12.61	0.39		0.49 ($p < 0.01$)	–
Anterior width: inter-incisive	2.43	0.04	2.45	0.08	2.51	0.06	2.50	0.07	0.53 ($p < 0.01$)		–
Middle width: inter-masseteric ridge	5.53	0.06	5.61	0.11	5.43	0.12	5.41	0.11	0.82 ($p < 0.01$)		–
Posterior width: inter-coronoid	11.27	0.13	11.30	0.23	10.24	0.66	10.40	0.67	0.48 ($p < 0.001$)		–
Posterior width: inter-condylar	11.28	0.19	11.23	0.22	11.05	0.34	10.95	0.32	1.04 ($p < 0.01$)		–
Posterior width: inter-gonial	11.76	0.24	11.52	0.36	12.22	0.34	11.72	0.68	0.41 ($p < 0.05$)	0.45 ($p < 0.05$)	–
Dental feature: first molar teeth									0.86 ($p < 0.001$)	ns	6.00 ($p < 0.001$)
Maxilla											
Height: CEJ–MB cusp tip (buccal)	0.77	0.03	0.76	0.03	0.74	0.04	0.73	0.06	0.28 ($p < 0.05$)[a]	ns	2.20 ($p < 0.001$)[d]
Length: mesio-distal (buccal)	1.95	0.03	1.94	0.04	1.91	0.04	1.93	0.27	0.24 ($p < 0.05$)[b]	ns	3.26 ($p < 0.001$)[e]
Width: bucco-palatal (occlusal)	1.03	0.02	1.02	0.02	1.10	0.04	1.10	0.05	0.79 ($p < 0.001$)[c]	ns	3.32 ($p < 0.001$)[f]
Mandible											
Height: CEJ–ML cusp tip (lingual)	0.93	0.06	0.93	0.04	0.91	0.03	0.92	0.04	0.28 ($p < 0.05$)[a]	ns	2.20 ($p < 0.001$)[d]
Length: mesio-distal (lingual)	1.76	0.04	1.72	0.04	1.71	0.04	1.71	0.03	0.24 ($p < 0.05$)[b]	ns	3.26 ($p < 0.001$)[e]
Width: bucco-lingual (occlusal)	0.83	0.04	0.82	0.05	0.86	0.04	0.86	0.04	0.79 ($p < 0.001$)[c]	ns	3.32 ($p < 0.001$)[f]

Abbreviation: ns = non-significant ($p > 0.05$).
Maxillary and mandibular skeletal measurements (n = 10).
Maxillary and mandibular tooth measurements (n = 20).
Two-way MANOVA showed significant effects of genotype and sex on skeletal features (maxillary-zygomatico-temporal region as well as mandible). Three-way MANOVA showed significant effects of genotype and jaw on tooth dimensions.
For the skeletal features, p values with grey shadowing show SC < WT and M < F whereas those with clear background show SC > WT and M > F.
For dental features of the first molar teeth, p values with grey shadowing show SC < WT[a,b] and Mx > Mn[e,f] whereas those values with clear background show SC > WT[c] and Mx < Mn[d].
All length and dental dimensions were measured bilaterally and averaged for statistical analysis.
Effect size (Cohen's f) and significance levels are presented for both the overall MANOVA models as well as individual parameters.
Effect size (Cohen's f) was calculated using the formula: $f = \sqrt{(\eta^2/(1-\eta^2))}$, where η^2 (partial ita-squared) values were MANOVA outputs from the SPSS software [the effect size (f) of 0.10 is mild, 0.25 is moderate and 0.40 is high].

matic arch, due to differing densities of bone present. However, the bony presence was confirmed with dissection, indicating hypoplasia or partial (incomplete) ossification in cranial bones (Fig. 4(a, b)). In the murine model of SCS, incompletely ossified temporal bone (unilateral or bilateral) was present in 4 (20%) of 20 of mice, incompletely ossified zygomatic arch in 5 (25%) mice and twisted and/or incompletely ossified palatal process of the maxilla, premaxilla and the ventral nasal concha in 8 (40%) of mice compared with no such presentation in wild-type.

3.2. Mandible

The descriptive statistics for mandibular parameters are summarised in Table 2 and Fig. 1(b, c). Two-way MANOVA showed significant effects of genotype (Wilks' $\lambda = 0.20$; hypothesis df = 10; error df = 27; F = 11.05; $p < 0.001$) and sex (Wilks' $\lambda = 0.33$; hypothesis df = 10; error df = 27; F = 5.48; $p < 0.001$) on mandibular dimensions. Compared with wild-type, mandibles in the Twist1$^{+/-}$ mice demonstrated these trends: *(i) height*: significantly shorter

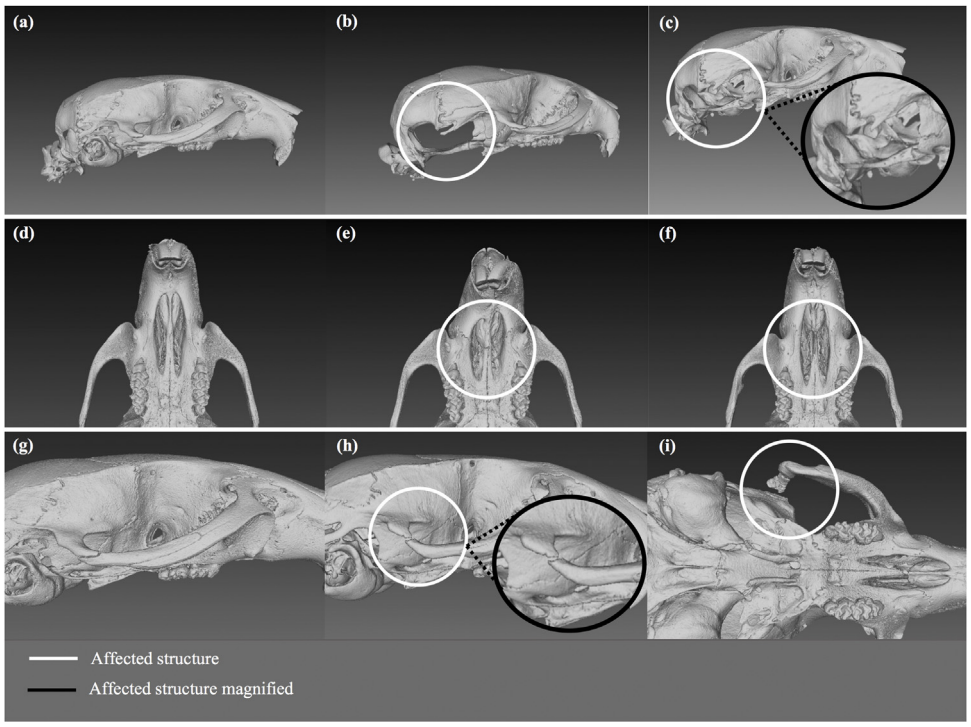

Fig. 3. Maxillary-zygomatico-temporal features of murine model of SCS (Twist1$^{+/-}$) in comparison to wild-type (Twist1$^{+/+}$) mice. The temporal bone (right view) was unaffected in Twist1$^{+/+}$ mice (a), seemingly absent around the tympanic and mastoid processes bilaterally (b) or unilaterally (c) in Twist1$^{+/-}$ mice. The palatal process of the maxilla, premaxilla and the ventral nasal concha (ventral view) was unaffected in Twist1$^{+/+}$ mice (d), twisted (e) or seemingly absent (f) in Twist1$^{+/-}$ mice. The zygomatic arch (right view) was unaffected in Twist1$^{+/+}$ mice (g), seemingly absent around the junction of the zygomatic bone and the zygomatic process of the temporal bone (h) or around the junction of the zygomatic process of the temporal bone and the temporal bone (i) in Twist1$^{+/-}$ mice (right inferior view for (i)).

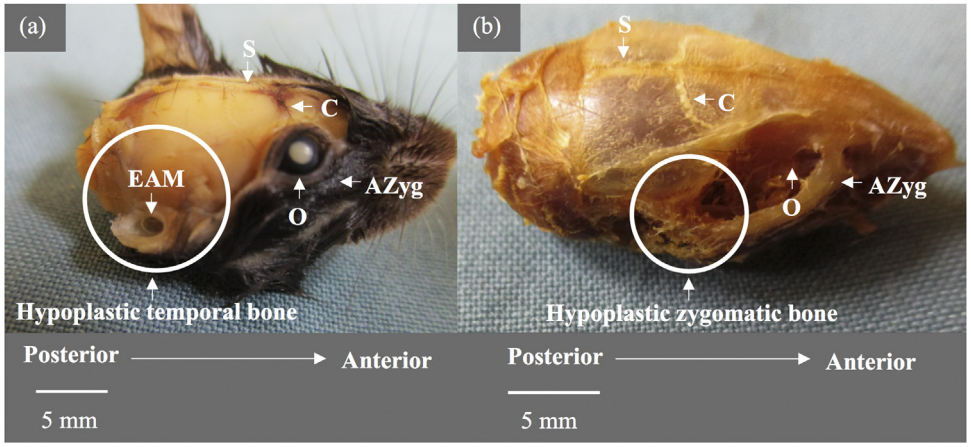

Fig. 4. Dissection images from the right oblique superior view of the temporal bone in a partially defleshed skull (a) and zygomatic arch in a completely defleshed skull (b) in the Twist1$^{+/-}$ murine model (same skull). These images correspond to the micro-CT images of in Fig. 3 (c and h, respectively) displaying seemingly absent temporal bone and discontinuity of the zygomatic process. The dissection revealed relatively intact temporal bone (white circle in (a)) and zygomatic process (white circle in (b)), indicating that these bones were only hypoplastic or partially (incompletely) ossified in the Twist1$^{+/-}$ mouse than grossly deformed (with missing parts). (Labels: anterior (A), posterior (P), zygomatic process of the maxilla (AZyg), orbit (O), external acoustic meatus (EAM), sagittal suture (S), coronal suture (C)).

ascending height (97.5% at $p < 0.05$), descending height (91.7% at $p < 0.001$) and anterior height (95.3% at $p < 0.001$), and unaltered posterior height ($p > 0.05$); *(ii) length*: unaltered mandibular length ($p > 0.05$); *(iii) width*: significantly longer anterior (inter-incisive) width (102.7% at $p < 0.01$), significantly shorter middle (inter-masseteric ridge) width (97.3% at $p < 0.01$), and complex alterations in posterior widths (i.e. significantly shorter inter-coronoid width (91.4% at $p < 0.001$); significantly shorter inter-condylar width (97.7% at $p < 0.01$), and significantly longer inter-gonial width (102.8% at $p < 0.05$)). Males displayed significantly larger mandibles than females for ascending height and posterior height (104.5% and 105.0% respectively at $p < 0.001$), mandibular length (102.3% at $p < 0.01$) and inter-gonial width (103.2% at $p < 0.05$). The effect size values for significant differences noted for the mandible were large to very large for both genotype (0.38–1.04) and sex (0.45 to 0.66) (Table 2). In the murine model of SCS, incidental findings of bifid coronoid processes were present in 14 (70%) of mice (Fig. 5(a–d)).

3.3. Teeth

These descriptive statistics for tooth parameters are summarised in Table 2 and Fig. 2(a–d). Three-way MANOVA showed

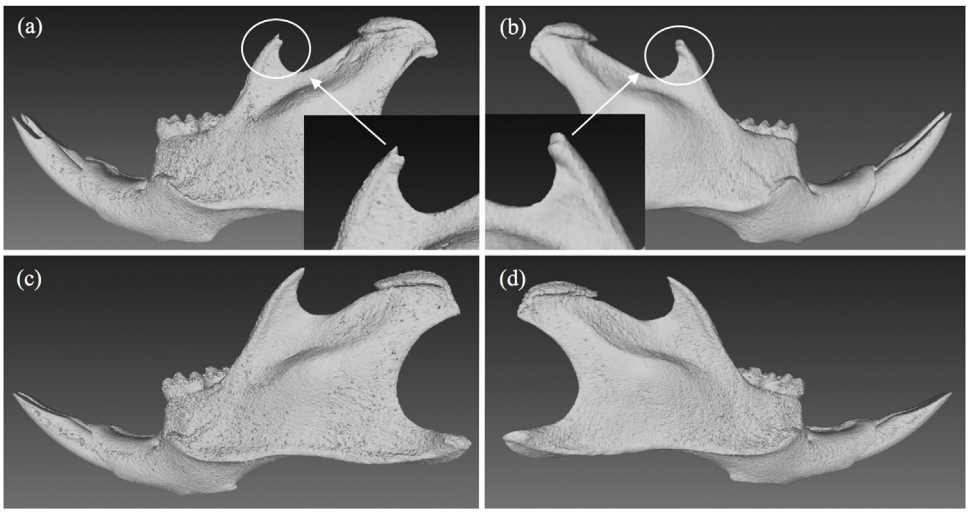

Fig. 5. Mandibular coronoid process in murine model of SCS (Twist1$^{+/-}$) in comparison to wild-type (Twist1$^{+/+}$) mice, specifically showing bifid coronoid processes in Twist1$^{+/-}$ mice (a, b) and unaffected coronoid processes in Twist1$^{+/+}$ mice (c, d). Images (a) and (c) represent the left buccal views and images (b) and (d) represent the right buccal views.

significant effects of genotype (Wilks' $\lambda = 0.76$, hypothesis df = 3, error df = 70, F = 7.4, $p < 0.001$) and jaw (Wilks' $\lambda = 0.01$, hypothesis df = 3, error df = 70, F = 1636.50, $p < 0.001$) on tooth parameter, but not of sex (Wilks' $\lambda = 0.94$, hypothesis df = 3, error df = 70, F = 1.56, $p > 0.05$). There was no significant interaction within the three parameters ($p > 0.05$). Compared with wild-type, dental crown measurements in the Twist1$^{+/-}$ mice (combined for both the maxilla and the mandible) demonstrated these trends: *(i) height (cementoenamel junction (CEJ) – mesiobuccal (MB) or mesiolingual (ML) cusp tip):* significantly shorter (97.2% at $p < 0.05$); *(ii) length (mesial to distal proximal surface at maximum convexity)*: significantly shorter (98.5% at $p < 0.05$) and *(iii) width (widest part of the occlusal table from the buccal to the lingual surfaces along the marginal ridge):* significantly longer (105.8% at $p < 0.001$). The effect size values for significant differences noted for the teeth were moderate to large for genotype (0.24–0.79) and jaw (2.20–3.32) (Table 2).

4. Discussion

We accept our hypothesis as the majority of the dimensions in the maxillary-zygomatico-temporal region and the mandible in the murine model of SCS (Twist1$^{+/-}$) were significantly shorter compared with wild-type. In the murine model of SCS, the maxillary-zygomatico-temporal region was significantly hypoplastic in length and posterior width, and the mandible demonstrated significant hypoplasia in height and width from the anterior molar region to the condylar area. Only one of four significant parameters for the maxillary-zygomatico-temporal region (i.e. middle inter-anterior zygomatic width), was larger in the murine model of SCS, which could have occurred by chance alone. Alternatively, this could be a reflection of localized overgrowth associated with Twist1$^{+/-}$ mutation in this region.

Changes in craniofacial morphogenesis have been linked to compensatory growth around sutures in craniosynostosis, in order to accommodate for the growing brain (Morriss-Kay and Wilkie, 2005). If this was true, the changes would be expected to occur exclusively in the craniofacial region. However, our findings of significantly smaller mandible in the murine model of SCS support the notion that the action of Twist1 extends beyond the skeletal structures directly affected by premature suture fusion (Parsons et al., 2014). Indeed, a conditional model of Twist1 inactivation during embryonic developmental has shown a wide range of anomalies in the frontonasal region, the maxilla and the proximal (posterior) part of the mandible in embryos due to skeletal differentiation in the neural crest-derived cells, along with indirect effects on mesenchymal precursors (via loss of interaction with neural crest cells) (Bildsoe et al., 2009). The molecular mechanism appears to involve extensive crosstalk between the Twist and FGF/FGFR signalling pathways to result in sutural bone overgrowth and premature suture fusion in craniosynostosis (Connerney et al., 2008). Loss of Twist1 gene has also been linked with reduced expression of Runx2 (which is transcription factor/master switch for osteogenesis), which is likely to affect osteoblastic differentiation, bone formation, skeletal morphogenesis and tooth formation (Bildsoe et al., 2009; Ratisoontorn et al., 2005; Seto et al., 2007). It seems that Twist1$^{+/-}$ mutation affects various craniofacial structures regardless of their embryonic origin (i.e. ectoderm, mesoderm, endoderm and NCCs) and further research is needed to clarify this.

Molecular therapies used to rescue phenotypes have been previously modelled through utilizing the interactions between different genes involved in syndromic craniosynostosis. For example, the introduction of Twist1 null alleles to Runx2 deficient mice can rescue a hypoplastic phenotype. A similar approach with Twist1 has the potential to become a future viable treatment option to correct craniofacial phenotypes in syndromic craniosynostosis specific to Twist1 haploinsufficiency (Lee et al., 2019). Dentally, previous research has suggested that smaller incisors and molars may be compensatory to hypoplastic jaws (Zhang et al., 2012), and our data of reduced length of the maxilla coupled with significantly shorter mesio-distal crown length of the first maxillary molar partly supports this hypothesis. However, our findings of significantly longer bucco-lingual dental crown widths relative to both smaller maxillary and medial mandibular skeletal widths implies a relatively greater effect of the gene expression on tooth development than on jaw development in the transverse plane.

Twist1$^{+/-}$ murine models have been associated with shortened cranial base and this could have resulted in a hypoplastic maxillary-zygomatico-temporal complex (Parsons et al., 2014). Consequently, this may have affected mandibular morphogenesis to produce hypoplastic mandible around the condylar and alveolar regions. The two significantly larger mandibular dimensions in the murine model of SCS compared with wild-type, i.e. the inter-incisive and the inter-gonial widths, may represent regions either being unaffected by maxillary hypoplasia (as they are not in direct articulation with the maxilla) or localised overgrowth from Twist1$^{+/-}$ mutation. Changes to the cranial base are not unique to SCS, and shortened

cranial base has also been linked to Apert-, Crouzon- and Pfeiffer syndrome, with the aetiology being attributed to gene mutation.

Alteration in the temporal bone, zygomatic arch, palatal process of the maxilla, premaxilla and the ventral nasal concha, and bifid coronoid processes in our murine model of SCS (Figs. 3 and 4) relate to reduced mineralization or delayed ossification due to Twist1 haploinsufficiency. Twist1 is an established mediator in bone development and ossification, including endochondral and intramembranous (Bialek et al., 2004; Yousfi et al., 2002; Zhang et al., 2012). For example, human SCS studies have shown delayed bone age due to the impaired action of Twist1 (Anderson et al., 1996; Trusen et al., 2003). Our observation of incomplete ossification of the tympanic and mastoid processes of the temporal bone are consistent with previous reports of delayed ossification of the tympanic ring and adjacent structures in murine model of SCS (Bourgeois et al., 1998; Zhang et al., 2012). Bifid coronoid processes observed in our murine model of SCS could be another manifestation of an ossification defect in mutated mice. Although this feature has not been reported in humans affected by the SCS, they have been associated with delayed ossification in other conditions, such as chronic AsA deficiency in Osteogenic Disorder Shionogi (rat) (Sakamoto and Takano, 2002). The functional implication of bifid coronoid process remains unknown. As the temporalis muscle and coronoid process are intimately related (i.e. the coronoid processes develops from within the temporalis muscle), it is possible that alterations to the muscle during development or function may influence the coronoid process (Auvenshire, 2017). However, further research is required to understand the associations between bifid coronoid processes, temporal muscle activity, size and attachment and mandibular movement.

In relation to sexual dimorphism, five skeletal parameters were significantly larger in males than females for the maxillary-zygomatico-temporal region and the mandible (Table 2). However, sexual dimorphism was not observed in dental parameters. There are currently no high level human studies confirming sexual dimorphism in patients with SCS. Therefore, it is difficult to ascertain whether sexual dimorphism in skeletal structures is determined by the action of sex hormones (androgen and oestrogen), the X and Y chromosomes, GH-IGF-1, or Twist1$^{+/-}$ (Alvesalo, 2009; Callewaert et al., 2010). Twist1 suppresses Runx2 expression, which has transcription control over its downstream factor aromatase that is required for synthesis of sex hormones (androgens and oestrogens) (Jeong and Choi, 2011; Öz et al., 2000). It would therefore appear fruitful to study the effect of sex hormones in the presence of Twist1 haploinsufficiency.

Our results for the murine model of SCS are generally consistent with previous observations using murine models, including compromised skeletogenic differentiation of the maxilla in conditional Twist1 knockout mouse embryos (Bildsoe et al., 2009) and snout torsion in neonatal Twist1$^{+/-}$ mice (Bourgeois et al., 1998). Our observation of mandibular hypoplasia in height and width (except for intergonial width) also supports previous observations of shortened mandibles of Twist mutant embryos (Chen and Behringer, 1995; da Fontoura et al., 2015). Nonetheless, some features of murine models have not been reported in human models, including bifid coronoid processes in murine model of SCS in the present study and bifid condylar processes in Crouzon mice in a previous study (Khominsky et al., 2018). It appears that certain gene signalling pathways in craniofacial syndrome may not be fully conserved between humans and mice. Alternatively, differences between human and mice growth trajectories and early intervention in humans may account for the observed variations.

Future phenomics studies using conditional Twist1 models, which allow for gene inactivation at different developmental times and tissue specific locations, would broaden the understanding of the temporospatial impact of Twist1 in the craniofacial region. Without this understanding, we cannot attribute craniofacial changes to the action of Twist1 alone or previously hypothesized compensatory mechanisms. Geometric morphometric techniques could be useful to elucidate shape changes in the cranium and the teeth using approaches described recently (Parsons et al., 2014; Yong et al., 2018). With greater understanding of craniofacial phenomics, the findings may extend into gene therapy and combined surgical and pharmaceutical management. For example, Bariana et al. (2017a, 2017b) have explored alternative treatments for craniosynostosis and identified the potential of Titania nanotube-based cranial implants as a vector to administer pharmacological agents. Phenotypic studies are now driving the development of novel therapeutic intervention in conditions such as stroke (Lanktree et al., 2010), heart failure (Shah et al., 2014), Parkinson's and Alzheimer's disease (Toga et al., 2015) and a similar approach could be translated to SCS management.

5. Conclusions

We conclude that the maxillary-zygomatico-temporal region and mandible were overall smaller in an SCS murine model (Twist1$^{+/-}$) compared with the wild-type (Twist1$^{+/+}$). Specifically, the maxillary-zygomatico-temporal region was significantly reduced in length and posterior width and the mandible was significantly reduced in height and width from the anterior molar region to the condylar area. These effects are reflective of the direct effects of the Twist1$^{+/-}$ mutation in the craniofacial region and they also affected the dental parameters. The maxillary and mandibular teeth were reduced in height (CEJ–DB cusp tip), reduced in length (mesiodistally) and increased in width (buccolingually). The murine model of SCS also displayed incompletely ossified temporal bone and zygomatic arch, twisted and/or incompletely ossified palatal process of the maxilla, premaxilla and the ventral nasal concha, and bifid coronoid processes. Overall, our data provide a sound basis for future research especially as we envision the move towards molecular intervention in the management of craniosynostosis.

Ethical statement

Stated in Section 2 of the manuscript:

Ethics approval was obtained from the University of Adelaide and the Women's and Children's Health Network (WCHN) Animal Ethics Committee (AEC 1001) (approval number 1000/8/2018).

Acknowledgments

The authors would like to acknowledge the support of the Australian Dental Research Foundation, the Australian Craniomaxillofacial Foundation, Ruth Williams from Adelaide Microscopy and the Women's and Children's Hospital (Adelaide) for housing the animal colony.

Funding

This work was supported by the Australian Dental Research Foundation Inc. (ADRF 195-2017) and the Australian Cranio-Maxillo Facial Foundation (ACMFF).

References

Alvesalo, L., 2009. Human sex chromosomes in oral and craniofacial growth. Arch. Oral Biol. 54, S18–S24.

Anderson, P.J., Hall, C.M., Evans, R.D., Hayward, R.D., Jones, B.M., 1996. The hands in Saethre-Chotzen syndrome. J. Craniofac. Genet. Dev. Biol. 16, 228–233.

Auvenshire, R.C., 2017. Embryology of the masticatory system. In: Gremillion, H.A., Klasser, G.D. (Eds.), Temporomandibular Disorders: a Translational Approach

from Basic Science to Clinical Applicability. Springer International Publishing AG, Cham, pp. 3–16.
Bariana, M., Dwivedi, P., Ranjitkar, S., Kaidonis, J.A., Losic, D., Anderson, P.J., 2017a. Biological response of human suture mesenchymal cells to Titania nanotube-based implants for advanced craniosynostosis therapy. Colloids Surf. B Biointerfaces 150, 59–67.
Bariana, M., Dwivedi, P., Ranjitkar, S., Kaidonis, J.A., Losic, D., Anderson, P.J., 2017b. Titania nanotube-based glypican delivery system to regulate BMP2 bioactivity in C2C12 cells for craniosynostosis therapy. Nanomedicine 17, 30111–30119.
Bialek, P., Kern, B., Yang, X., Schrock, M., Sosic, D., Hong, N., Wu, H., Yu, K., Ornitz, D.M., Olson, E.N., Justice, M.J., Karsenty, G., 2004. A twist code determines the onset of osteoblast differentiation. Dev. Cell 6, 423–435.
Bildsoe, H., Loebel, D.A., Jones, V.J., Chen, Y.T., Behringer, R.R., Tam, P.P., 2009. Requirement for Twist1 in frontonasal and skull vault development in the mouse embryo. Dev. Biol. 331, 176–188.
Bildsoe, H., Fan, X., Wilkie, E.E., Ashoti, A., Jones, V.J., Power, M., Qin, J., Wang, J., Tam, P.P., Loebel, D.A., 2016. Transcriptional targets of TWIST1 in the cranial mesoderm regulate cell-matrix interactions and mesenchyme maintenance. Dev. Biol. 418, 189–203.
Bourgeois, P., Bolcato-Bellemin, A.L., Danse, J.M., Bloch-Zupan, A., Yoshiba, K., Stoetzel, C., Perrin-Schmitt, F., 1998. The variable expressivity and incomplete penetrance of the twist-null heterozygous mouse phenotype resemble those of human Saethre-Chotzen syndrome. Hum. Mol. Genet. 7, 945–957.
Callewaert, F., Sinnesael, M., Gielen, E., Boonen, S., Vanderschueren, D., 2010. Skeletal sexual dimorphism: relative contribution of sex steroids, GH–IGF1, and mechanical loading. J. Endocrinol. 207, 127–134.
Carver, E.A., Oram, K.F., Gridley, T., 2002. Craniosynostosis in Twist heterozygous mice: a model for Saethre-Chotzen syndrome. Anat. Rec. 268, 90–92.
Chen, Z.F., Behringer, R.R., 1995. Twist is required in head mesenchyme for cranial neural tube morphogenesis. Genes Dev. 9, 686–699.
Cignoni, P., Callieri, M., Corsini, M., Dellepiane, M., Ganovelli, F., Ranzuglia, G., 2008. MeshLab: an open-source mesh processing tool. In: The Sixth Eurographics Italian Chapter Conference., pp. 129–136.
Connerney, J., Andreeva, V., Leshem, Y., Mercado, M.A., Dowell, K., Yang, X., Lindner, V., Friesel, R.E., Spicer, D.B., 2008. Twist1 homodimers enhance FGF responsiveness of the cranial sutures and promote suture closure. Dev. Biol. 318, 323–334.
da Fontoura, C.S., Miller, S.F., Wehby, G.L., Amendt, B.A., Holton, N.E., Southard, T.E., Allareddy, V., Moreno Uribe, L.M., 2015. Candidate gene analyses of skeletal variation in malocclusion. J. Dent. Res. 94, 913–920.
Epstein, C.J., Erickson, R.P., Wynshaw-Boris, A.J., 2004. Inborn errors of development: the molecular basis of clinical disorders of morphogenesis. In: Ew, J. (Ed.), TWIST and the Saethre-Chotzen Syndrome. Oxford University Press, New York.
Flaherty, K., Singh, N., Richtsmeier, J.T., 2016. Understanding craniosynostosis as a growth disorder. WIREs Dev. Biol. 5, 429–459.
El Ghouzzi, V., Lajeunie, E., Le Merrer, M., Cormier-Daire, V., Renier, D., Munnich, A., Bonaventure, J., 1999. Mutations within or upstream of the basic helix-loop-helix domain of the TWIST gene are specific to Saethre-Chotzen syndrome. Eur. J. Hum. Genet. 7, 27–33.
Harris, E.F., Smith, R.N., 2009. Accounting for measurement error: a critical but often overlooked process. Arch. Oral Biol. 54 (Suppl. 1), S107–S117.
Jeong, J.H., Choi, J.Y., 2011. Interrelationship of Runx2 and estrogen pathway in skeletal tissues. BMB Rep. 44, 613–618.
Khominsky, A., Yong, R., Ranjitkar, S., Townsend, G., Anderson, P.J., 2018. Extensive phenotyping of the orofacial and dental complex in Crouzon syndrome. Arch. Oral Biol. 86, 123–130.
Kress, W., Schropp, C., Lieb, G., Petersen, B., Büsse-Ratzka, M., Kunz, J., Reinhart, E., Schäfer, W.D., Sold, J., Hoppe, F., Pahnke, J., Trusen, A., Sörensen, N., Krauss, J., Collmann, H., 2006. Saethre-Chotzen syndrome caused by TWIST 1 gene mutations: functional differentiation from Muenke coronal synostosis syndrome. Eur. J. Hum. Genet. 14, 39–48.
Lanktree, M.B., Dichgans, M., Hegele, R.A., 2010. Advances in genomic analysis of stroke: what have we learned and where are we headed? Stroke 41, 825–832.
Lee, K.K.L., Stanier, P., Pauws, E., 2019. Mouse model of syndromic craniosynostosis. Mol. Syndromol. 10, 58–73.
Meng, T., Huang, Y., Wang, S., Zhang, H., Dechow, P.C., Wang, X., Qin, C., Shi, B., D'Souza, R.N., Lu, Y., 2015. Twist1 is essential for tooth morphogenesis and odontoblast differentiation. J. Biol. Chem. 290, 29593–29602.
Mian, M., Ranjitkar, S., Townsend, G.C., Anderson, P.J., 2017. Alterations in mandibular morphology associated with glypican 1 and glypican 3 gene mutations. Orthod. Craniofac. Res. 20, 183–187.
Morriss-Kay, G.M., Wilkie, A.O., 2005. Growth of the normal skull vault and its alteration in craniosynostosis: insights from human genetics and experimental studies. J. Anat. 207, 637–653.
O'Rourke, M.P., Tam, P.P., 2004. Twist functions in mouse development. Dev. Biol. 46, 401–413.
Öz, O.K., Zerwekh, J.E., Fisher, C., Graves, K., Nanu, L., Millsaps, R., Simpson, E.R., 2000. Bone has a sexually dimorphic response to aromatase deficiency. J. Bone Miner. Res. 15, 507–514.
Parsons, T.E., Weinberg, S.M., Khaksarfard, K., Howie, R.N., Elsalanty, M., Yu, J.C., Cray Jr., J.J., 2014. Craniofacial shape variation in Twist1+/− mutant mice. Anat. Rec. 297, 826–833.
Ratisoontorn, C., Seto, M.L., Broughton, K.M., Cunningham, M.L., 2005. In vitro differentiation profile of osteoblasts derived from patients with Saethre-Chotzen syndrome. Bone 36, 627–634.
Richtsmeier, J.T., Baxter, L.L., Reeves, R.H., 2000. Parallels of craniofacial maldevelopment in down syndrome and Ts65Dn mice. Dev. Dyn. 217, 137–145.
Sakamoto, Y., Takano, Y., 2002. Morphological influence of ascorbic acid deficiency on endochondral ossification in osteogenic disorder Shionogi rat. Anat. Rec. 268, 93–104.
Seto, M.L., Hing, A.V., Chang, J., Hu, M., Kapp-Simon, K.A., Patel, P.K., Burton, B.K., Kane, A.A., Smyth, M.D., Hopper, R., Ellenbogen, R.G., Stevenson, K., Speltz, M.L., Cunningham, M.L., 2007. Isolated sagittal and coronal craniosynostosis associated with TWIST box mutations. Am. J. Med. Genet. A 143A, 678–686.
Shah, S.J., Katz, D.H., Selvaraj, S., Burke, M.A., Yancy, C.W., Gheorghiade, M., Bonow, R.O., Huang, C.C., Deo, R.C., 2014. Phenomapping for novel classification of heart failure with preserved ejection fraction. Circulation 131, 269–279.
Stoler, J.M., Rogers, G.F., Mulliken, J.B., 2009. The frequency of palatal anomalies in Saethre-Chotzen syndrome. Cleft Palate Craniofac. J. 46 (3), 280–284.
Taylor, J.A., Bartlett, S.P., 2017. What's new in syndromic craniosynostosis surgery? Plast. Reconstr. Surg. 140, 82e–93e.
Toga, A.W., Foster, I., Kesselman, C., Madduri, R., Chard, K., Deutsch, E.W., Price, N.D., Glusman, G., Heavner, B.D., Dinov, I.D., Ames, J., Van Horn, J., Kramer, R., Hood, L., 2015. Big biomedical data as the key resource for discovery science. J. Am. Med. Inform. Assoc. 22, 1126–1131.
Trusen, A., Beissert, M., Collmann, H., Darge, K., 2003. The pattern of skeletal anomalies in the cervical spine, hands and feet in patients with Saethre-Chotzen syndrome and Muenke-type mutation. Pediatr. Radiol. 33, 168–172.
Twigg, S.R., Wilkie, A.O., 2015. A genetic-pathophysiological framework for craniosynostosis. Am. J. Hum. Genet. 97, 359–377.
Wang, J.C., Nagy, L., Demke, J.C., 2016. Syndromic craniosynostosis. Facial Plast. Surg. Clin. North Am. 24, 531–543.
Woods, R.H., Ul-Haq, E., Wilkie, A.O., Jayamohan, J., Richards, P.G., Johnson, D., Lester, T., Wall, S.A., 2009. Reoperation for intracranial hypertension in TWIST1 confirmed Saethre-Chotzen syndrome: a 15 year review. Plast. Reconstr. Surg. 123, 1801.
Yong, R., Ranjitkar, S., Lekkas, D., Halazonetis, D., Evans, A., Brook, A., Townsend, G., 2018. Three-dimensional (3D) geometric morphometric analysis of human premolars to assess sexual dimorphism and biological ancestry in Australian populations. Am. J. Phys. Anthropol. 166, 373–385.
Yousfi, M., Lasmoles, F., Kern, B., Marie, P.J., 2002. TWIST inactivation reduces CBFA1/RUNX2 expression and DNA binding to the osteocalcin promoter in osteoblasts. Biochem. Biophys. Res. Commun. 297, 641–644.
Zhang, Y., Blackwell, E.L., McKnight, M.T., Knutsen, G.R., Vu, W.T., Ruest, L.B., 2012. Specific inactivation of Twist1 in the mandibular arch neural crest cells affects the development of the ramus and reveals interactions with hand2. Dev. Dyn. 241, 924–940.